

Gold Nanoelectrodes of Varied Size: Transition to Molecule-Like Charging

Shaowei Chen, Roychelle S. Ingram, Michael J. Hostetler, Jeremy J. Pietron, Royce W. Murray,* T. Gregory Schaaff, Joseph T. Khoury, Marcos M. Alvarez, Robert L. Whetten*

A transition from metal-like double-layer capacitive charging to redox-like charging was observed in electrochemical ensemble Coulomb staircase experiments on solutions of gold nanoparticles of varied core size. The monodisperse gold nanoparticles are stabilized by short-chain alkanethiolate monolayers and have 8 to 38 kilodaltons core mass (1.1 to 1.9 nanometers in diameter). Larger cores display Coulomb staircase responses consistent with double-layer charging of metal-electrolyte interfaces, whereas smaller core nanoparticles exhibit redox chemical character, including a large central gap. The change in behavior is consistent with new near-infrared spectroscopic data showing an emerging gap between the highest occupied and lowest unoccupied orbitals of 0.4 to 0.9 electron volt.

Nanoparticles of metals and semiconductors have sparked intense interest (1) in anticipation that this unexplored range of materials dimensions will yield size-dependent optical, electronic, and chemical properties suitable for applications in optoelectronic nanodevices, catalysts, and chemical sensors (2–4). Among known preparations of nanoparticles (5–8), recent attention has focused on alkanethiolate monolayer-protected metal clusters (MPCs). Gold MPCs in particular are quite stable and can be prepared with average core diameters of 1.1 to 5 nm. Electrochemical studies have demonstrated that Au MPCs are equivalent to diffusing, nanometer-sized electrodes (9) and can provide electrocatalytic advantages (10). Further, room-temperature solutions of MPCs with monodisperse cores display an electrochemical “ensemble Coulomb staircase” (11), a behavior anticipated and explained based on the sub-attofarad double-layer capacitances (C_{CLU}) of diffusing, nanometer-sized 28-kD metallic Au particles coated with a monolayer (hexanethiolate, C6) dielectric. Analogous staircase phenomena have been reported, using nanometer-sized electrodes (12).

We aim to further understand electrochemical ensemble Coulomb staircases by varying the monodisperse core mass in Au MPC solutions from 8 to 38 kD (core diameters of 1.1 to 1.9 nm). The double-layer capacitive charging seen for larger core sizes

changes for smaller MPC core sizes to a molecular redox-like behavior. That is, over a certain range of core sizes, electron orbital-shell effects or pairing effects, or both, begin to dominate, changing the cluster capacitance from one determined by electrostatic processes to one more dominated by bonding interactions.

Coulomb staircases for nanoparticles are usually observed as tunneling currents through a single nanoparticle addressed by a tip probe (Fig. 1A), that undergo stepwise increments with increasing tip-substrate bias (V) (13, 14). A model accounting for junction capacitances in a double tunnel-junction circuit (Fig. 1A) predicts that current increments occur at critical voltage biases (V_C)

$$V_C = Ze/C + (1/C)(Q_0 + e/2) \quad (1)$$

where Z is integral nanoparticle charge, e the electron charge, C capacitance of the more resistive junction, and Q_0 a fraction associated with tip-substrate work function differences. Coulomb staircase charging is normally observed at low temperatures because of the requirement that the stepwise charging energy ($E_C = e^2/C$) greatly exceeds thermal energy, $k_B T$, where k_B is Boltzmann's constant and T is temperature. Equation 1 predicts that if C is constant, consecutive charging steps should occur at a regular spacing $\Delta V_C = e/C$.

Figure 1, C and D, presents electrochemical ensemble Coulomb staircase behavior for MPCs of varied core mass, in the form of differential pulse voltammograms (DPVs) at a Pt electrode. The interfacial double-layer chargings of the uniform electronic charge and core-size MPCs with C4 and C6 coatings (15) produce a series of DPV current peaks (in both positive- and negative-scan directions) that occur at the $\Delta V_C =$

6. A. C. Redfield, *Am. Sci.* **46**, 205 (1958).
7. N_2 fixation was estimated by acetylene reduction [R. J. Flett, R. D. Hamilton, N. E. R. Campbell, *Can. J. Microbiol.* **22**, 43 (1976)] on liquid samples melted slowly. Incubations were at 1°C and 100 μmol of photons $\text{m}^{-2} \text{s}^{-1}$ for 20 to 36 hours. A conversion factor of 0.33 (moles of N_2 fixed per mole of C_2H_2 produced) was used to estimate N_2 fixation rates from ethylene production.
8. The vertical offset between microbial biomass and activity maxima in Fig. 1, C and D, reflects variation between core samples and core length used for the analyses (14-cm core sections were used for data in Fig. 1, A to C; 30-cm sections were used for data in Fig. 1D). Because sediment aggregates occurred in relatively compact layers, rates would be higher if measured on shorter core sections incorporating the sediment layer only.
9. Lyophilized sediments for confocal microscopy were stained with 4',6'-diamidino-2-phenylindole (DAPI) (1 mg ml^{-1}) and examined on a Leica laser scanning confocal microscope. Microautoradiography [H. W. Paerl and E. A. Stull, *Limnol. Oceanogr.* **24**, 1166 (1979)] was performed on slowly melted ice-core samples incubated at 4°C for 8 hours with ^{14}C -labeled bicarbonate (0.5 $\mu\text{Ci ml}^{-1}$) at 100 μmol of photons $\text{m}^{-2} \text{s}^{-1}$.
10. DNA was extracted from sediments in the lake ice with guanidinium isothiocyanate [D. G. Pitcher, N. A. Saunders, R. J. Owen, *Lett. Appl. Microbiol.* **8**, 151 (1989)]. Bacterial 16S ribosomal RNA primers 27F and 1522R [D. J. Lane, in *Nucleic Acid Techniques in Bacterial Systematics*, E. Stackebrandt and M. Goodfellow, Eds. (Wiley, New York, 1991), pp. 115–148] were used for the polymerase chain reaction (PCR) [R. K. Saiki *et al.*, *Science* **239**, 487 (1988)]. The amplicons were cloned into the vector PCR II (Invitrogen) and bidirectionally sequenced with dye terminator chemistry on an ABI 377 automated sequencer (Applied Biosystems, Foster City, CA). The tree in Fig. 3 was inferred from a sequence mask of 966 positions by the neighbor-joining [N. Saitou and M. Nei, *Mol. Biol. Evol.* **4**, 406 (1987)] and parsimony methods [J. Felsenstein, *PHYLIIP* (University of Washington, Seattle, 1991)].
11. J. C. Priscu and H. W. Paerl, data not shown.
12. G. D. Clow, C. P. McKay, R. A. Simmons Jr., *J. Clim.* **7**, 715 (1988).
13. K. T. Wing and J. C. Priscu, *Antarct. J. U.S.* **28**, 246 (1993).
14. C. H. Fritsen and J. C. Priscu, *J. Phycol.* **34**, 493 (1998).
15. Wind-blown sediment deposits were quantified during early September before direct sunlight reached the lake. Sediments from within 100- m^2 quadrants were collected and weighed; subsamples were analyzed for POC with an elemental analyzer. These surface sediments represent aeolian deposition that had accumulated before direct sunlight and elevated temperatures induced melting when winds were highest in the area (12). Wind-blown sediment deposition is highest during this period [J. C. Priscu *et al.*, unpublished data] and provides an estimate of annual deposition. Replicate sediment traps (22.5-cm opening) containing 5% formalin were deployed beneath the ice for 1 year. Collected sediments were rinsed, dried, and weighed. A sediment portion was acidified with 6 M HCl, redried, and analyzed for POC.
16. C. H. Fritsen, V. I. Lytle, S. F. Ackley, C. W. Sullivan, *Science* **266**, 782 (1994).
17. M. Felip, B. Sattler, R. Psenner, J. Catalan, *Appl. Environ. Microbiol.* **61**, 2394 (1995).
18. C. P. McKay, E. I. Friedmann, R. A. Wharton, W. L. Davies, *Adv. Space Res.* **12** (no. 4), 231 (1992).
19. C. P. McKay and C. R. Stoker, *Rev. Geophys.* **27**, 189 (1989).
20. M. J. S. Belton *et al.*, *Science* **274**, 377 (1996).
21. G. W. Ojakangas and D. J. Stevenson, *Icarus* **81**, 220 (1989).
22. M. H. Carr *et al.*, *Nature* **391**, 363 (1998).
23. We thank T. Meuwissen for field assistance. Supported by the NSF (OPP 94-19423 and OPP 92-11773).

S. Chen, R. S. Ingram, M. J. Hostetler, J. J. Pietron, R. W. Murray, Department of Chemistry, Kenan Laboratories, University of North Carolina, Chapel Hill, NC 27599–3290, USA.

T. G. Schaaff, J. T. Khoury, M. M. Alvarez, R. L. Whetten, Schools of Chemistry and Physics, Georgia Institute of Technology, Atlanta, GA 30332–0430, USA.

*To whom correspondence should be addressed. E-mail: rwm@email.unc.edu (R.W.M.) or robert.whetten@physics.gatech.edu (R.L.W.)

2 March 1998; accepted 20 April 1998

e/C_{CLU} spacings summarized in Fig. 2. The MPCs reach and depart the electrode/solution interface by diffusion, so that the sizes of the current peaks are determined by a series of interfacial electron-transfer and diffusional (“Warburg”) impedances (Fig. 1B). A very large number of MPCs become charged during each DPV peak, being those forming the diffusion layer around the electrode, hence our use (11) of the term “ensemble staircase.”

The DPV peak spacings for the larger MPC core sizes (22, 28, and 38 kD) differ from those of the smaller ones (8 and 14 kD). Figure 2 shows that the central ΔV_C spacings [solid brackets, peaks spanning $E = 0$ V where Z is nearest zero (16)] are similar (0.32 to 0.40 V) for the larger core sizes and correspond to $C_{CLU} = 0.4$ to 0.5 aF/cluster, or 3 to 4 $\mu\text{F}/\text{cm}^2$ when normalized for estimated Au core surface areas (A_{CLU}). These values are similar to capacitances (C_{DL}) of macroscopic alkanethiolate monolayer-coated Au(111) surfaces (17) and to average C_{DL} 's of polydisperse MPC solutions (9). Also, the ΔV_C spacings for the larger core MPCs (Fig. 2) decrease slightly at more positive and negative E , as expected for double-layer capacitances. Thus, the DPV results for the larger MPC core sizes in Fig. 1, C and D, and Fig. 2 can be confidently interpreted as charging of metal cores coated with a dielectric film and in an electrolyte solution.

For the smaller core MPCs (8 and 14 kD), however, the central ΔV_C spacings [1.2 and 0.7 V, Fig. 2, solid brackets (18)] are much larger than the central ΔV_C spacings of the larger core MPCs. They are also much larger than the ΔV_C spacings seen at more positive and negative E , for both small- and large-core MPCs (Fig. 2, dotted brackets). Further, only minor changes in C_{CLU} are expected from changes in A_{CLU} , based on consideration of the concentric sphere capacitance model (9) and given the similarities of core radii to monolayer dielectric thicknesses. The qualitatively different voltammetric behavior of the 8- and 14-kD MPCs is highly reminiscent of redox transformations known for Pt-carbonyl clusters [Pt_n(CO)_m, $n = 24, 26,$ and 38] (19). Thus, the results in Fig. 1, C and D, and Fig. 2 show, within a series of MPCs of nominally constant architecture and composition, a transition from classical metal-like double-layer charging to that resembling electrochemical charging of an electroactive molecule.

The core-size dependent change in Fig. 1, C and D, and Fig. 2 suggest the emergence of a significantly quantized electron-level structure, including, for example, the appearance of a substantial gap between the highest occupied and lowest unoccupied orbitals (HOMO-LUMO) in the neutral (or

as obtained) clusters. Such a gap should also be manifest in their optical spectroscopic responses, which are shown in Fig. 3 for three of the above MPCs, along with (for comparison) a larger MPC (66 kD, ~ 2.2 nm) and bulk (colloidal) Au. The response function ϵ_2 (imaginary part of the complex dielectric function) reflects the density and strength of optical transitions at each transition energy and shows several strong trends with decreasing MPC core size: (i)

enhanced strength in the near-infrared region (<1.8 eV), (ii) the appearance of discrete or band-like spectral features, and (iii) an increasing “gap” energy, reflecting primarily the HOMO-LUMO gap, below which (in contrast to the ω^{-3} divergence of bulk Au) the optical response vanishes. For the 28-kD MPC, the gap is no greater than 0.4 eV (the smallest energy for which the functions are reliable), but the 14- and 8-kD MPCs exhibit larger gaps, estimated as 0.6

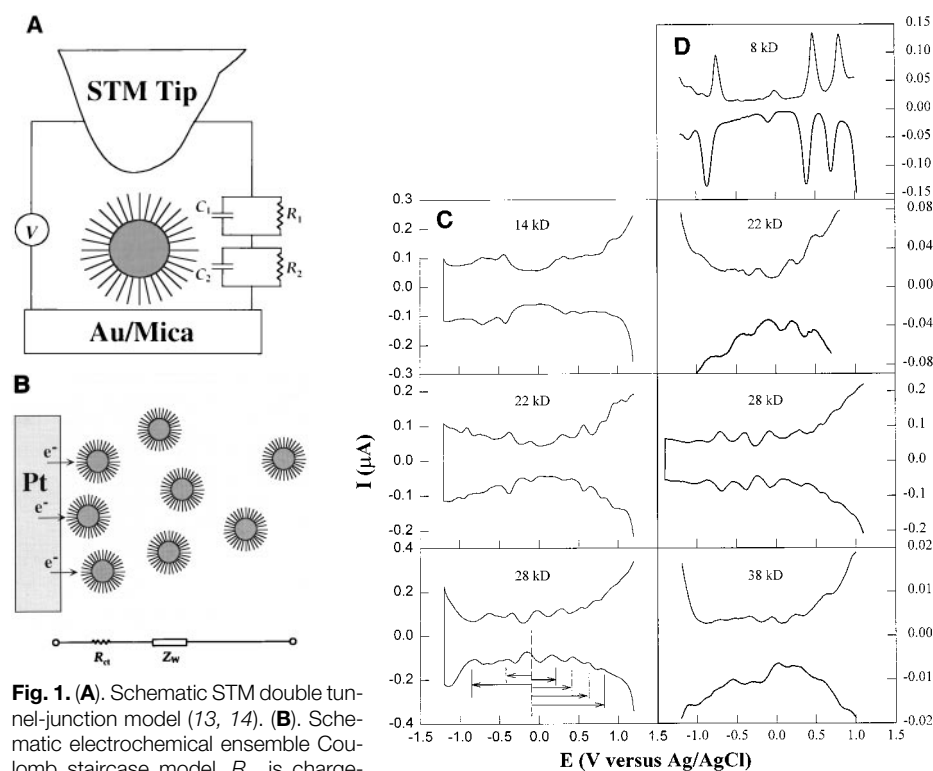


Fig. 1. (A) Schematic STM double tunnel-junction model (13, 14). (B) Schematic electrochemical ensemble Coulomb staircase model. R_{ct} is charge-transfer resistance and Z_w is diffusional (Warburg) impedance for MPC transport through the solution. Differential pulse voltammograms for (C) butanethiolate (C4) and (D) hexanethiolate (C6) Au MPCs as a function of uniform core size, in 0.05 M Hex₄NClO₄/toluene/acetonitrile (2/1 v:v), at 9.5×10^{-3} cm² Pt electrode; DC potential scan 10 mV/s, pulse amplitude 50 mV. Concentrations are: (C) 14 kD, 0.086 mM; 22 kD, 0.032 mM; 28 kD, 0.10 mM; (D) 8 kD, 0.30 mM; 22 kD, 0.10 mM; 28 kD, 0.10 mM; 38 kD, 0.10 mM. Arrows at lower left indicate ΔE potential steps used in Fig. 4.

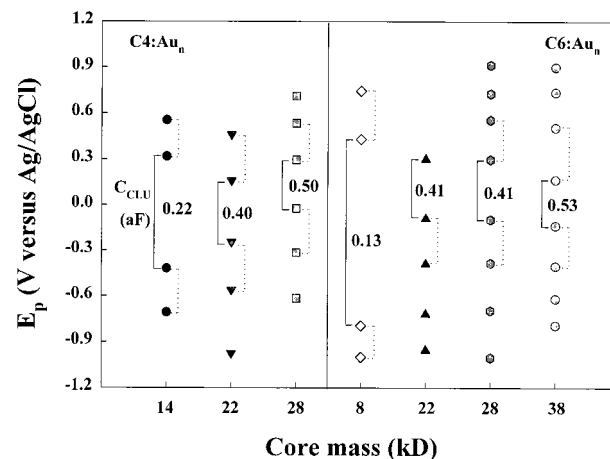


Fig. 2. DPV peak potentials for MPCs in Fig. 1, C and D. C_{CLU} values are shown for the ΔV_C nearest $E = 0$ V (solid line brackets), those for adjacent ΔV_C spacings are shown by dotted brackets. For the large-core MPCs, the C_{CLU} values correspond to a monolayer dielectric constant of about 5.

and nearly 0.9 eV, respectively. These gaps are reasonable in terms of the electronic structure of Au clusters, which have all of the gross characteristics of the bulk

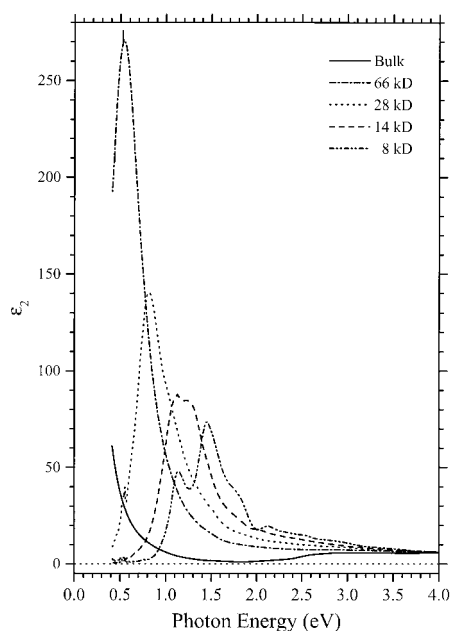
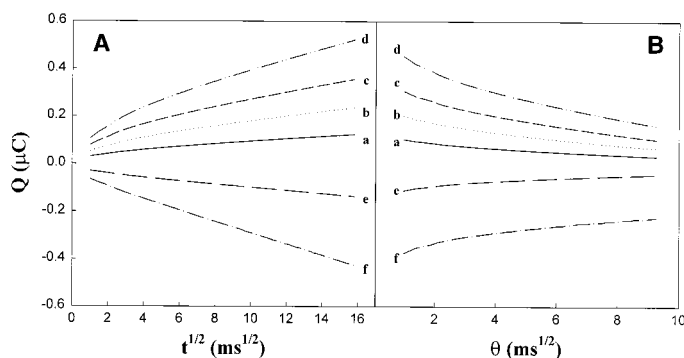


Fig. 3. Optical response (ϵ_2) of monodisperse Au MPCs with various core sizes. The HOMO-LUMO gaps vary with core size: (a) bulk Au, 0 eV; (b) 66 kD, $\ll 0.4$ eV; (c) 28 kD, $\ll 0.4$ eV; (d) 14 kD, ~ 0.6 eV; (e) 8 kD, ~ 0.9 eV. These curves were derived from a dispersion analysis (Kramers-Kronig relation) of the optical absorbance spectra, across the 0.2 to 6.4 eV range, of dilute solutions at room temperature. Absorbances at lower energies were obtained by extrapolating measured spectra and those in the far UV by assuming convergence to bulk Au values. Dielectric functions (ϵ_1 and ϵ_2) of the (assumed spherical) nanoparticles were computed from absorption coefficients and calculated index of refraction using a model of the effective dielectric constants for the nanoparticle-medium composite (Mie theory), as was done in (8).

Fig. 4. Plots for forward (A; $t < \tau$) and reverse (B; $t > \tau$) steps in double potential step chronocoulometry for C4, 28 kD MPC solution (steps shown by arrows in Fig. 1, C and D, lower left). Step reversal time 0.25 s. (a) Slopes ($C/ms^{1/2}$) for smallest (-0.103 V \leftrightarrow 0.200 V) forward and reverse potential step are, respectively, $S_F = 5.1 \times 10^{-9}$ and $S_R = -5.68 \times 10^{-9}$. Using this S_F in Eq. 1 with $D = 1.54 \times 10^{-6}$ cm²/s (from microelectrode voltammetry) gives $C_{CLU} = 0.55$ aF, which is close to that obtained from $\Delta V_C = e/C_{CLU}$ (0.50 aF, Fig. 2) where $1e^-$ transfer is assumed. Normalizing slopes for the other forward and reverse potential steps to S_F and S_R gives (b) -0.106 V \leftrightarrow 0.400 V, 2.0 S_F , 2.0 S_R ; (c) -0.100 V \leftrightarrow 0.600 V, 2.9 S_F , 3.0 S_R ; (d) -0.092 V \leftrightarrow 0.800 V, 4.4 S_F , 4.3 S_R ; (e) -0.090 V \leftrightarrow -0.420 V, $-1.3 S_F$, $-0.8 S_R$; (f) -0.090 V \leftrightarrow -0.800 V, $-4.6 S_F$, $-1.9 S_R$. The forward slope for the -0.090 V \leftrightarrow -0.800 V step is enlarged by reduction of solution O_2 impurity.



bands for clusters with more than 20 atoms (20), assuming that clusters with closed electron shells are preferentially formed and isolated. The differences between the spectroscopic gaps and electrochemical ΔV_C values (0.74 and 1.2 eV, respectively) for the 14- and 8-kD cores are explainable considering that the spectroscopic values are estimated as band edges, whereas the ΔV_C results are taken at the DPV peak maxima, not their edges. A similar electrochemical/orbital-energy correlation has been found for Pt-carbonyl clusters (19) and also for C_{76} fullerene (21) and La@ C_{82} metallofullerene (22), but in those cases, no higher homologs were available to observe the transition to the double-layer capacitive charging that occurs for the larger Au MPCs.

That the DPV peaks of Fig. 1, C and D, all correspond to $1e^-$ transfers is supported by double potential step chronocoulometry of a C4, 28-kD MPC solution. Figure 4 shows charge-time results from stepping E from its rest value (approximately -0.1 V versus a Ag/AgCl electrode) by ΔE to the valleys between successive DPV peaks (Fig. 1, C and D, lower left, see arrows), and back. The equation for diffusion-controlled charging of MPCs in the forward potential step is (23)

$$Q = \frac{2\Delta E C_{CLU} A D^{1/2} C^*}{\pi^{1/2}} t^{1/2} + Q_{ADS} + Q_{DL} \quad (2)$$

The back potential step equation has an analogous time dependence (23) and the same slope terms. Calculating C_{CLU} from the slope S_F of the smallest forward ΔE step (-0.103 V \leftrightarrow 0.200 V) chronocoulometric plot in Fig. 4 gives a value (0.55 aF) close to that obtained from the central ΔV_C spacing

(0.50 aF) in DPV, as expected for both being $1e^-$ transfers. That the other DPV peaks are also $1e^-$ transfers is shown by Fig. 4, in that the slopes of forward and back plots change by integral multiples of those (S_F and S_R , respectively) of the smallest ΔE step (-0.103 V \leftrightarrow 0.200 V, assuming constant C_{CLU}) as ΔE is incremented across successive charging peaks.

Finally, although the analogy between electrochemical ensemble and classical Coulomb staircase charging is strong, there are differences worth noting. (i) Their equivalent circuits differ as shown in Fig. 1, A and B, the principal reason being that the electrochemical currents are controlled by MPC diffusion. (The equivalent circuits would be more alike were the MPCs attached as a monolayer to the electrode.) (ii) The capacitance (C_{CLU}) that determines ΔV_C spacings in the electrochemical case is that of the entire MPC surface, whereas capacitance in the classical experiment (Fig. 1A) is determined by the two junction contacts. (iii) The electrochemical case involves an ensemble of MPCs (as opposed to a single nanoparticle in Fig. 1A), so that macroscopic transport relations can be used to describe their voltammetry, as illustrated in Fig. 4. (iv) It is difficult to conceive of a fractionally charged MPC in solution, so there is no analogy in electrochemical ensemble charging to Q_O in Eq. 1.

Solution-phase electrochemical ensemble Coulomb staircase charging has also been observed in experiments performed on arylthiolated Au MPCs, so our results may be forerunners of a general phenomenon. In addition, because the staircase behavior is closely related to MPC core electronic energy structure, it may aid understanding of other nanophase properties, such as the metal-insulator transition of Ag nanoparticles upon compression (24). Finally, although differences in fundamental properties reside in the metal-like and molecule-like charging behaviors, we anticipate that their electrochemical, thermodynamic, and kinetic properties will, upon further study, prove to fit within a common formal representation.

REFERENCES AND NOTES

1. Proceedings of the Robert A. Welch Foundation 40th Conference on Chemical Research, *Chemistry on the Nanoscale*, 21 to 22 October 1996, Houston, TX (Robert A. Welch Foundation, Houston, TX, 1996).
2. G. Schmid, Ed., *Clusters and Colloids* (VCH, Weinheim, Germany, 1994).
3. M. A. Hayat, Ed., *Colloidal Gold: Principles, Methods, and Applications* (Academic Press, San Diego, CA, 1991).
4. R. Elghariani, J. J. Storhoff, R. C. Mucic, R. L. Letsinger, C. A. Mirkin, *Science* **277**, 1078 (1997).
5. M. Brust, M. Walker, D. Bethell, D. J. Schiffrin, R.

- Whyman, *J. Chem. Soc. Chem. Commun.* **1994**, 801 (1994).
6. M. J. Hostetter and R. W. Murray, *Curr. Opin. Colloid Interface Sci.* **2**, 42 (1997).
 7. R. L. Whetten *et al.*, *Adv. Mater.* **8**, 428 (1996); A. Badia *et al.*, *Chem. Eur. J.* **2**, 359 (1996).
 8. M. M. Alvarez *et al.*, *J. Phys. Chem. B* **101**, 3706 (1997); S. Underwood and P. Mulvaney, *Langmuir* **10**, 3427 (1994).
 9. S. J. Green, J. J. Stokes, M. J. Hostetter, J. J. Pietron, R. W. Murray, *J. Phys. Chem. B* **101**, 2663 (1997).
 10. R. S. Ingram and R. W. Murray, unpublished results.
 11. R. S. Ingram *et al.*, *J. Am. Chem. Soc.* **119**, 9279 (1997).
 12. F.-R. F. Fan and A. J. Bard, *Science* **277**, 1791 (1997).
 13. E. Hartmann, P. Marquardt, J. Ditterich, P. Radojkovic, H. Steinberger, *Appl. Surf. Sci.* **107**, 197 (1996); T. Sato and H. Ahmed, *Appl. Phys. Lett.* **70**, 2759 (1997); L. Guo, E. Leobandung, S. Y. Chou, *Science* **275**, 649 (1997); R. P. Andres *et al.*, *ibid.* **272**, 1323 (1996).
 14. M. Amman, R. Wilkins, E. Ben-Jacob, P. D. Maker, R. C. Jaklevic, *Phys. Rev. B* **43**, 1146 (1991); W. Hofstetter and W. Zwerger, *Phys. Rev. Lett.* **78**, 3737 (1997).
 15. These MPCs were prepared and separated as described previously [T. G. Schaaff *et al.*, *J. Phys. Chem. B* **101**, 7885 (1997)], with discrete core-sizes specified by core-mass (or equivalent core diameter or approximate number of Au atoms) as 8 kD (1.1 nm, ~38 Au atoms), 14 kD (1.35 nm, ~75), 22 kD (~1.5 nm, ~110), 28 kD (1.65 nm, ~145), and 38 kD (~1.8 nm, ~200), with a saturation monolayer coverage of butanethiolate (C4) or hexanethiolate (C6).
 16. AC impedance measurements, in the same solvent, on a monolayer of C4 28-kD MPCs chemically attached to a Au electrode surface reveal a shallow capacitance minimum at -0.2 V, which we take to be the potential of zero charge. The pzc for the unattached C4 clusters should be the same or very similar.
 17. M. D. Porter, T. B. Bright, D. L. Allara, C. E. D. Chidsey, *J. Am. Chem. Soc.* **109**, 3559 (1987).
 18. The minor peak near 0 V for the 8-kD MPC is thought to be an impurity due to nonuniform C_{CLU} or initial charge.
 19. J. D. Roth *et al.*, *J. Am. Chem. Soc.* **114**, 6159 (1992); M. J. Weaver and X. Gao, *J. Phys. Chem.* **97**, 332 (1993).
 20. K. J. Taylor, C. L. Pettiette-Hall, O. Cheshnovsky, R. E. Smalley, *J. Chem. Phys.* **96**, 3319, (1992).
 21. Q. Li, F. Wudl, C. Thilgen, R. L. Whetten, F. Diederich, *J. Am. Chem. Soc.* **114**, 3994 (1992).
 22. T. Suzuki *et al.*, *ibid.* **115**, 11006 (1993).
 23. In Eq. 2, F is Faraday constant, A is electrode area, D and C^* are MPC diffusion coefficient and concentration, respectively, Q_{ADS} is charging of any adsorbed MPC, and Q_{DL} is electrode double-layer charging. For the reverse step, $t^{1/2}$ is replaced by θ , that is, $(\tau^{1/2} + (t - \tau)^{1/2} - t^{1/2})$ where τ is the step reversal time [A. J. Bard and L. R. Faulkner, Eds., *Electrochemical Methods: Fundamentals and Applications* (Wiley, New York, 1980), chap. 5].
 24. C. P. Collier, R. J. Saykally, J. J. Shiang, S. E. Henrichs, J. R. Heath, *Science* **277**, 1978 (1997).
 25. Supported in part by grants from NSF (R.W.M., R.L.W.) and the U.S. Office of Naval Research (R.W.M.).

24 February 1998; accepted 13 May 1998

Giant Electrostriction and Relaxor Ferroelectric Behavior in Electron-Irradiated Poly(vinylidene fluoride-trifluoroethylene) Copolymer

Q. M. Zhang,* Vivek Bharti, X. Zhao

An exceptionally high electrostrictive response (~4 percent) was observed in electron-irradiated poly(vinylidene fluoride-trifluoroethylene) [P(VDF-TrFE)] copolymer. The material exhibits typical relaxor ferroelectric behavior, suggesting that the electron irradiation breaks up the coherent polarization domain (all-trans chains) in normal ferroelectric P(VDF-TrFE) copolymer into nanopolar regions (nanometer-size, all-trans chains interrupted by trans and gauche bonds) that transform the material into a relaxor ferroelectric. The expanding and contracting of these polar regions under external fields, coupled with a large difference in the lattice strain between the polar and nonpolar phases, generate an ultrahigh strain response.

Materials that generate large mechanical actuation induced by external stimuli including electric field, temperature, and stress have attracted a great deal of attention in recent years. The development goals include achieving a large range of motion with high precision and speed, high strain energy density to generate large forces, and a low fatigue rate for a long lifetime and high reliability. Although there are several active materials currently available, there are few that come close to meeting all of these goals. For instance, piezoceramic and magnetostrictive materials, although they have low hysteresis and fast speed, have low strain levels (~0.1%) (1, 2). Shape memory alloys generate high strain and high force but are often associated with large hysteresis and very slow speed (3).

Ferroelectric polymers, because they are easily processed, cheap, lightweight, and conform to complicated shapes and surfaces, have been studied for nearly three decades for applications in electromechanical devices (4, 5). However, the low strain level (~0.1%) and strain energy density of current ferroelectric polymers have severely limited their usefulness in these applications.

It should be noted that there is an important class of phenomena that has not been exploited in ferroelectric polymers for electromechanical applications: the large lattice strain and large dimensional change associated with phase transformations in these materials. One such example is poly(vinylidene fluoride), PVDF, and its random copolymer with trifluoroethylene, P(VDF-TrFE), which are the best known and most widely used ferroelectric polymers (4, 5). PVDF and its copolymer P(VDF-TrFE) are semicrystalline polymers that have a morphology of crystallites in an

amorphous surrounding. With proper sample treatments a ferroelectric phase (β phase, which has an all-trans conformation as shown in Fig. 1) can be induced in these polymers in the crystalline region (6). In compositions of P(VDF-TrFE) copolymers that exhibit a ferroelectric-paraelectric (F-P) transition (conversion of all-trans chains to a mixture of trans and gauche bonds), large lattice strains and sample dimensional changes (~10%) have been observed in x-ray diffraction and thermal expansion experiments (6-8). One drawback of this large strain associated with the transition is the large hysteresis (6-8).

It is well known that the existence of hysteresis in ferroelectric materials is due to the energy barrier when switching from one polarization direction to another or when transforming from one phase to another. In ferroelectric ceramic materials, the energy barrier can be significantly reduced or eliminated by reduction of the size of coherent polarization regions to a nanometer scale (9). In P(VDF-TrFE) copolymers, one possible approach to achieve this result (reduction of the size of all-trans conformation regions) is to introduce defects into the polymer chains. This may be accomplished with high-energy radiation. The influence of high-energy electrons and gamma irradiation on the dielectric and structural prop-

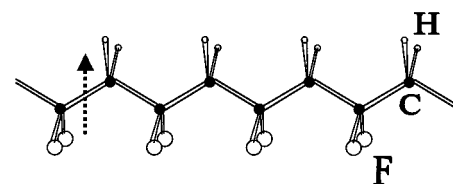


Fig. 1. Schematic depiction of the all-trans chain conformation in PVDF. The arrow indicates the dipole direction.

Materials Research Laboratory and Department of Electrical Engineering, Pennsylvania State University, University Park, PA 16802, USA.

*To whom correspondence should be addressed.